AD-A138 736 FEASIBILITY STUDIES OF OPTICAL PROCESSING OF IMAGE BANDWIDTH COMPRESSION SCHEMES(U) ARIZONA UNIV TUCSON B R HUNT ET AL. 15 MAY 83 AFOSR-TR-84-0143 1/1

UNCLASSIFIED AFOSR-81-0170 F/G 20/6 NL

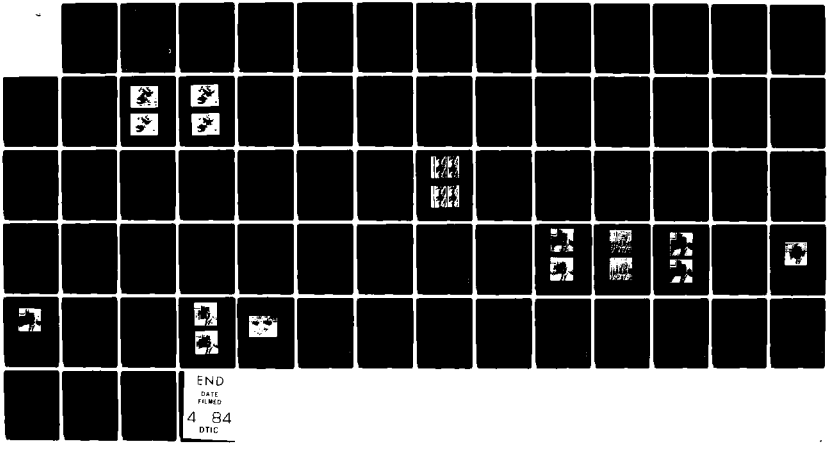

END
DATE FILMED
4 84
DTIC

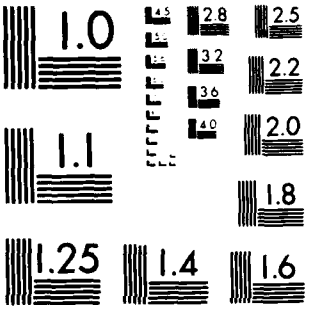

UNCLASSIFIED

SECURITY CLASSIFICATION OF THIS PAGE (When Data Entered)

(2)

REPORT DOCUMENTATION PAGE		READ INSTRUCTIONS BEFORE COMPLETING FORM
1. REPORT NUMBER AFOSR-TR- 84-0143	2. GOVT ACCESSION NO.	3. RECIPIENT'S CATALOG NUMBER
4. TITLE (and Subtitle) FEASIBILITY STUDIES OF OPTICAL PROCESSING OF IMAGE BANDWIDTH COMPRESSION SCHEMES		5. TYPE OF REPORT & PERIOD COVERED ANNUAL
		6. PERFORMING ORG. REPORT NUMBER
7. AUTHOR(s) B.R. HUNT R.N. STRICKIAND R.A. SCHOWENGERDT		8. CONTRACT OR GRANT NUMBER(s) AFOSR-81-0170
9. PERFORMING ORGANIZATION NAME AND ADDRESS Univ. of Arizona Tucson, Arizona 85721		10. PROGRAM ELEMENT, PROJECT, TASK AREA & WORK UNIT NUMBERS 61102F 2305/B1
11. CONTROLLING OFFICE NAME AND ADDRESS AFOSR/NE Bolling AFB, DC 20332		12. REPORT DATE MAY 15, 1983
		13. NUMBER OF PAGES 68
14. MONITORING AGENCY NAME & ADDRESS(if different from Controlling Office)		15. SECURITY CLASS. (of this report) UNCLASSIFIED
		15a. DECLASSIFICATION/DOWNGRADING SCHEDULE

16. DISTRIBUTION STATEMENT (of this Report)

APPROVED FOR PUBLIC RELEASE; DISTRIBUTION UNLIMITED

17. DISTRIBUTION STATEMENT (of the abstract entered in Block 20, if different from Report)

18. SUPPLEMENTARY NOTES

19. KEY WORDS (Continue on reverse side if necessary and identify by block number)

20. ABSTRACT (Continue on reverse side if necessary and identify by block number)

This research focuses on these three areas:
A) formulation of alternative architectural concepts for image bandwidth compression, i.e., the formulation of components and schematic diagrams which differ from conventional digital bandwidth compression schemes by being implemented by various optical computation methods;
B) simulation of optical processing concepts for image bandwidth compression, so as to gain insight into typical performance parameters and elements of

DD FORM 1 JAN 73 1473 EDITION OF 1 NOV 65 IS OBSOLETE UNCLASSIFIED (OVER)

SECURITY CLASSIFICATION OF THIS PAGE (When Data Entered)

20. (Cont.)

system performance sensitivity;

c) maturation of optical processing for image bandwidth compression until the overall state of optical methods in image compression becomes equal to that of digital image compression.

AFOSR-TR- 84-0143

Grant No. AFOSR-81-0170

Annual [redacted] Report

"Feasibility Studies of Optical Processing of Image Bandwidth Compression Schemes"

by

B. R. Hunt

R. N. Strickland

R. A. Schowengerdt

May 15, 1983

(I.) Introduction

Grant No. AFOSR-81-0170 has an objective which is well-summarized by the Grant title: "Feasibility studies of optical processing for image bandwidth compression schemes." It is the intent of research sponsored under this Grant to direct investigation into the following issues:

(a) formulation of alternative architechtural concepts for image bandwidth compression, i.e., the formulation of components and schematic diagrams which differ from conventional digital bandwidth compression schemes by being implemented by various optical computation methods;

(b) simulation of optical processing concepts for image bandwidth compression, so as to gain insight into typical performance parameters and elements of system performance sensitivity;

(c) maturation of optical processing for image bandwidth compression until the overall state of optical methods in image compression becomes equal to that of digital image compression.

It is the last of these, item (c), which represents the continuing strategic objective of the efforts being carried on under Grant No. AFOSR-81-0170. It is important to remember that the major attention given to image bandwidth compression has been for methods most conveniently implemented by digital computations. As flexible and multipurpose are digital methods, there

may always be operational circumstances, environments, or constraints where the availability of a different technology is important. However, with the concentration upon digital computations, which has characterized most research on bandwidth compression, alternative methods in optics have suffered. Thus, the purpose of research sponsored under this Grant is to serve as a source of alternatives for future concepts in bandwidth compression, so that the environment for compression technology need not be dominated by one methodology.

(II.) Overview of the Report

The research currently sponsored under Grant No. AFOSR-81-0170 consists of several distinct and separate activities. The separate research efforts are unified by a common theme: the application of optical processing for image bandwidth compression. Within this common theme, however, the separate research projects are not completely related to each other. Therefore, this report is put together, literally, as a number of independent reports. The separate sections of the report, which follow this section, are intended to be read separately and independently of any other section. Each section has its own references and its own figure labellings, for example.

The separate sections of this report, and the research problems dealt with in each section, are summarized in the following:

(1) Data compression by multi-spectral staggered sampling, and data reconstruction by spatial and spectral interpolation (see Section (III.)).

(2) Data compression by optical tomography, with data reconstruction by optical convolution and back projection (see Section (IV.)).

(3) Adaptive data compression by spatial transformations to create a spatially stationary image (see Section (V.)).

(4) Improvement of the optical data compression method known as IDPCM (see Section (VI.)).

(III.) Multispectral Staggered Sampling Data Compression

This section reviews progress on the project to achieve data compression of multispectral imagery by sensor undersampling and subsequent reconstruction of the original scene utilizing inter-band redundancy of edge information. The technique assumes that features possessing high spatial frequencies are similar in all spectral bands of a scene.

The sampling scheme considered in the present research consists of bands of a multispectral sensor which are under-sampled at staggered intervals in a scene. For example, the spatial arrangement of pixels in an equally-sampled four-band image, bands I-IV, is:

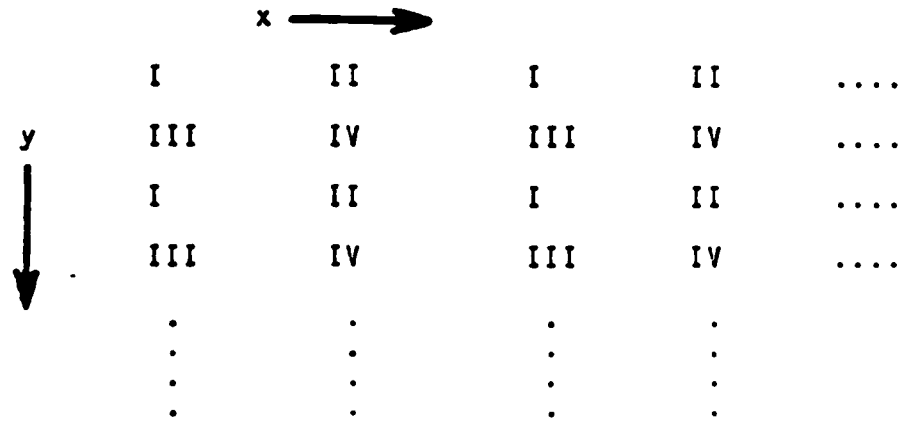

As shown in Figure 1, the pixels of this mosaic arrangement may be directly transmitted (PCM) for moderate data compression, or may be further encoded (eg. DPCM) for higher compression rates. At the receiver, DPCM decoding (if needed) is followed by re-construction of all pixels in each band. To accomplish this,

RECONSTRUCTION BY SPECTRAL REGRESSION

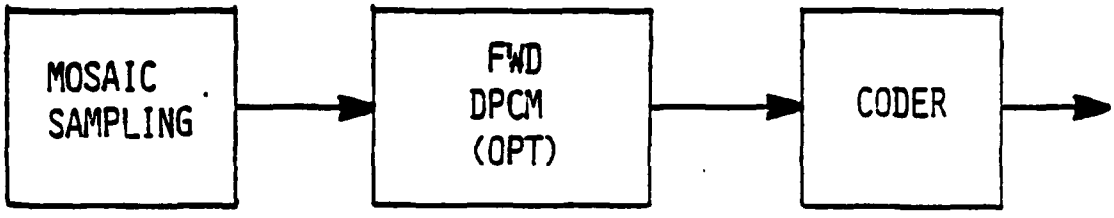

TRANSMITTER

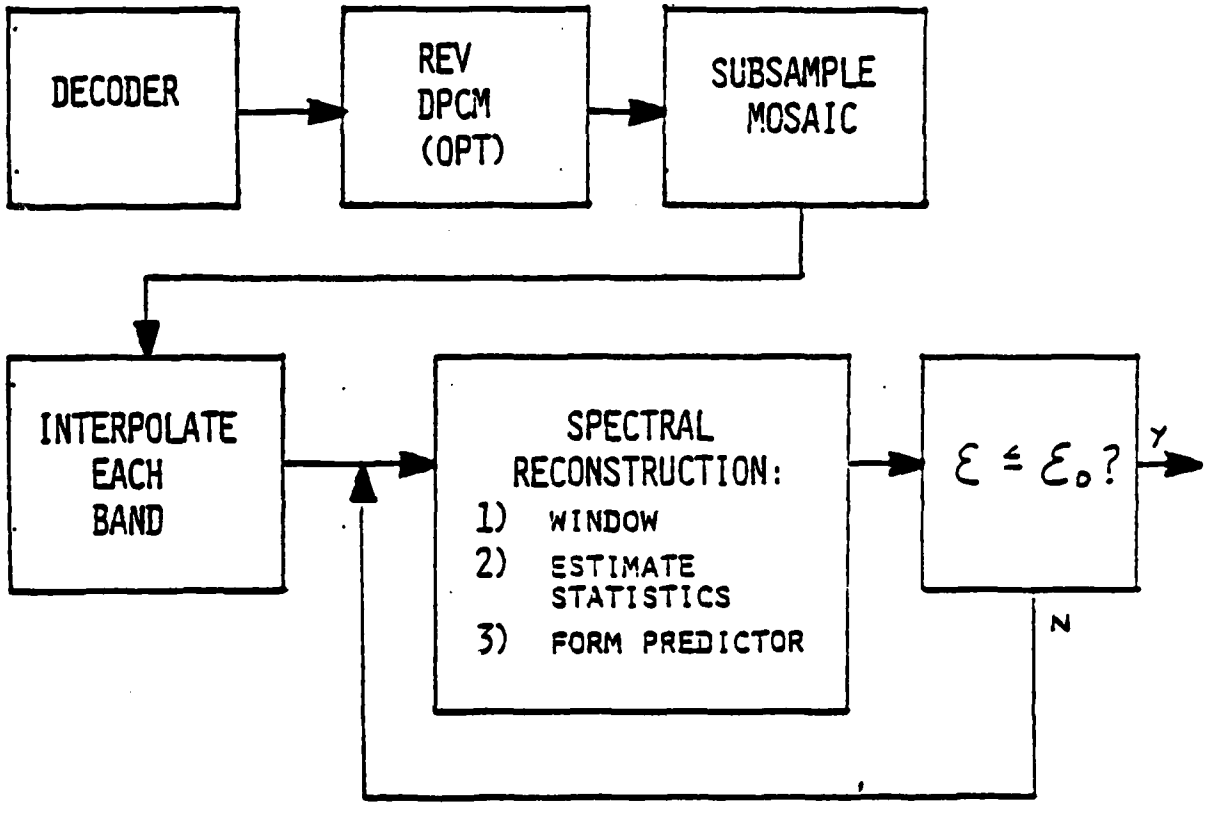

RECEIVER

Figure 1

the mosaic data is subsampled for each band in turn; these intra-band pixels are then spatially interpolated to the size of the full mosaic scene to become initial estimates in an iterative space-variant reconstruction using the spectral correlation between the bands.

The iteration scheme for reconstruction proceeds as follows. In each iteration, the pixels within a moving spatial window are used to calculate statistics needed in predictors of the missing bands. At each window location the center sample plus the predicted values are then written to corresponding spatial coordinates in four output images. The reconstruction is then either terminated or the reconstructions are used as approximate images in another iteration.

If E is the general band to be estimated, and S, F, G,. . . are the other bands sampled within the window, then an estimate of E could be formed from a linear prediction of all bands, i.e., $\hat{E} = \bar{E} + a\Delta S + b\Delta F + c\Delta G + \ldots$, where $\Delta S = S - \bar{S}$, etc. A MMSE criterion, such that $\langle (E-\hat{E})^2 \rangle$ is a minimum, results in the solution for the coupling parameters in terms of local band variances and spectral covariances:

$$\begin{bmatrix} a \\ b \\ c \\ \cdot \\ \cdot \\ \cdot \end{bmatrix} = \begin{bmatrix} s^2 & \langle \Delta S \Delta F \rangle & \langle \Delta S \Delta G \rangle \\ \langle \Delta S \Delta F \rangle & \sigma f^2 & \langle \Delta F \Delta G \rangle \\ \langle \Delta S \Delta G \rangle & \langle \Delta F \Delta G \rangle & \sigma g^2 \\ & \cdot & \\ & \cdot & \\ & \cdot & \end{bmatrix}^{-1} \begin{bmatrix} \langle \Delta E \Delta S \rangle \\ \langle \Delta E \Delta F \rangle \\ \langle \Delta E \Delta G \rangle \\ \cdot \\ \cdot \\ \cdot \end{bmatrix}$$

The band images will be treated as ergodic random processes over the extent of the estimation window, so that the ensemble averages are replaced by spatial averages.

Simulations

One-, two-, and three-band predictors have been tested in the reconstruction of a 256x256-pixel four-band LANDSAT MSS image. Bilinear interpolations of each band of the mosaic were used as initial estimates in the reconstruction. Figure 2 is a plot of normalized mean-square-error (NMSE) versus estimator window size for the second MSS band. The results are in agreement with two expected tendencies: larger variance in the statistical estimates are associated with decreasing window size; and higher-order predictors exhibit greater sensitivity to these statistical errors. For comparison, also plotted in Figure 2 are the results when the original images form the initial estimates. The reconsturction error increases with window size, reflecting the increasing nonstationarity within the window. It is seen that all spectral regressions result in significantly smaller error than does bilinear interpolation.

Without direct compression of the mosaic data, spectral regression reconstruction allows moderate data compression without compression hardware at the transmitter. Figure 3 is a plot of NMSE versus effective bit rate for 1st- and 2nd-order DPCM (using Laplacian quantization) of the LANDSAT image, compared with spectral regression and bilinear interpolation. At an effective bit rate of 7 bits/pixel ÷ 4 bands = 1.75 bits/pixel, spectral regression is numerically comparable in

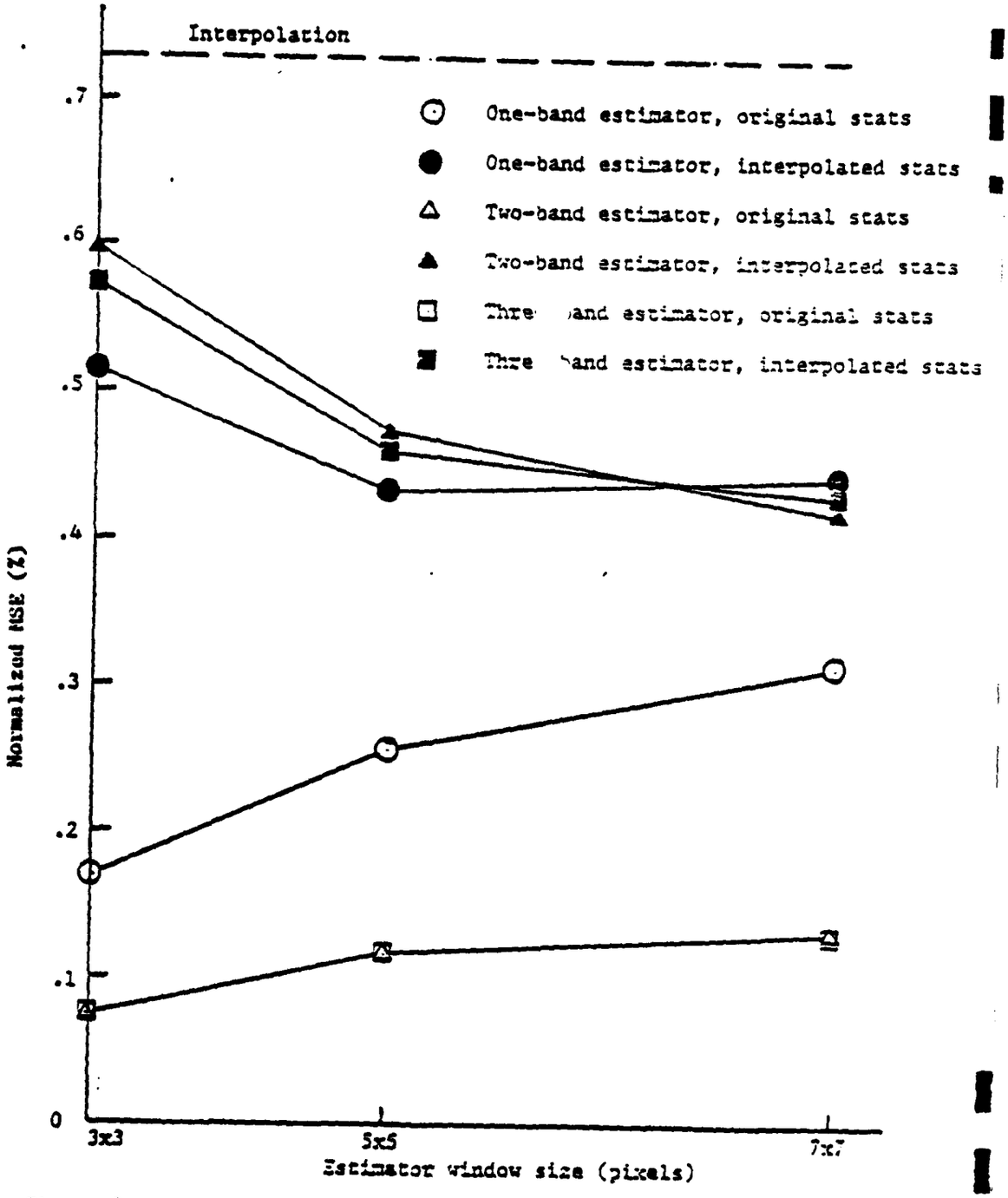

Figure 2. NMSE vs window size - Band 2.

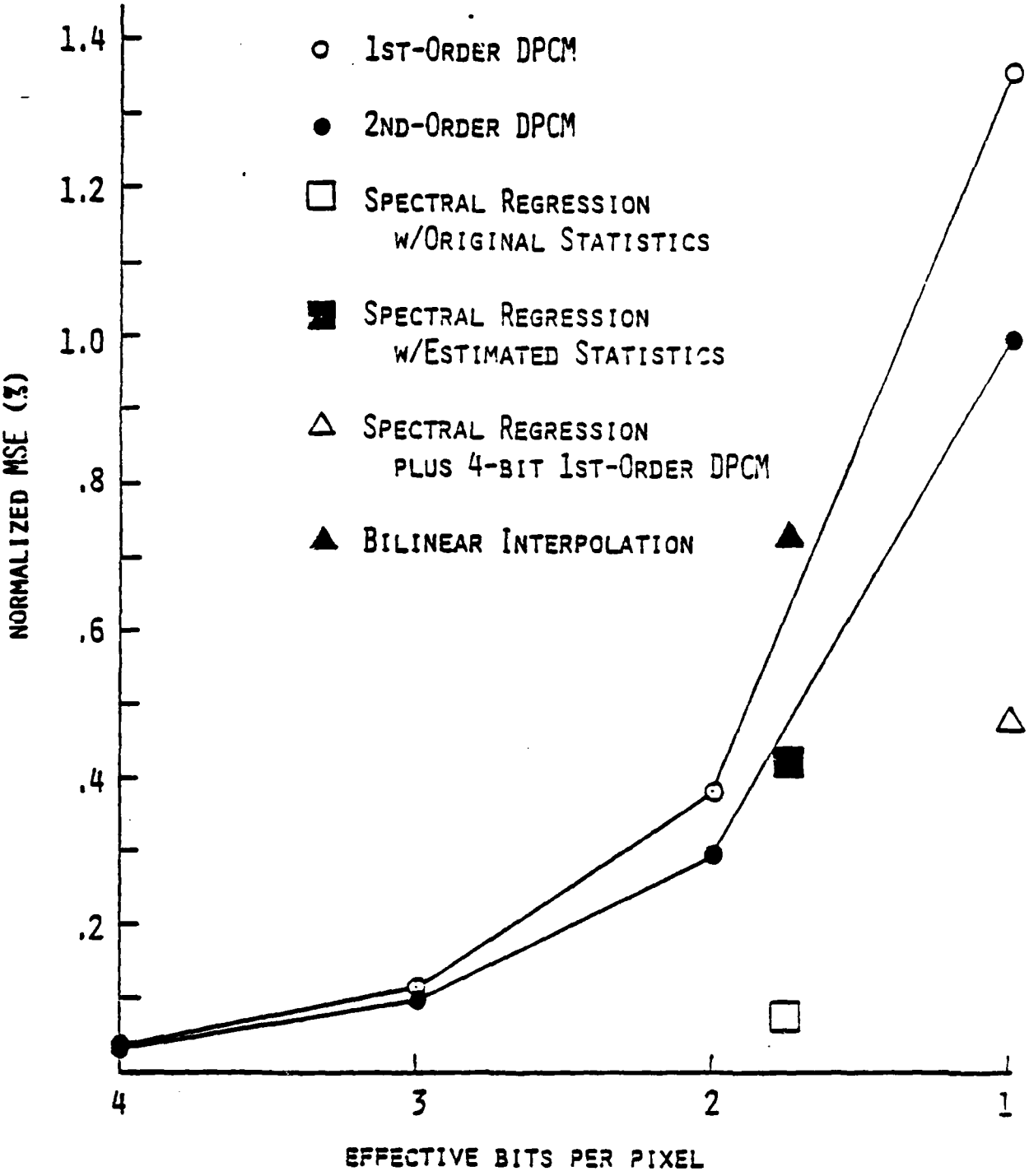

COMPARISON OF SPECTRAL REGRESSION WITH DPCM

NMSE VS. BIT RATE - BAND 2

Figure 3

accuracy to 2nd-order DPCM.

Further compression gains can be made in combining simple DPCM of the mosaic array with spectral regression. As shown in Figure 4, spectral regression with 1st-order mosaic DPCM is shown to be more accurate at 0.5 bits/pixel than direct 2nd-order DPCM at 1.0 bits/pixel. This is a significant performance gain.

The relative visual qualities of spectral regression and DPCM are demonstrated in Figures 5 - 8. Figure 5 is a detail photograph of the second MSS band original scene. The optimum 1st-order spectral regression over a 5 x 5 window at 1.75 bits/pixel is shown in Figure 6. By comparison, the 2nd-order DPCM reconstruction at 2 bits/pixel is given in Figure 7. The degradation in the regression case is primarily a random phasing in the low-contrast regions of the scene; the degradation in the DPCM case is chiefly granularity noise. Finally, mosaic DPCM with spectral regression at 0.5 bits/pixel is displayed in Figure 8.

Current research is examining the effects of scene spatial-frequency bandwidth and unequal band-sampling-rates on spectral regression performance.

Interim results of this research have been presented at the 1982 annual meeting of the Optical Society of America; a paper will also be presented at the August meeting of the Society of Photo-Optical Instrumentation Engineers in San Diego, California.

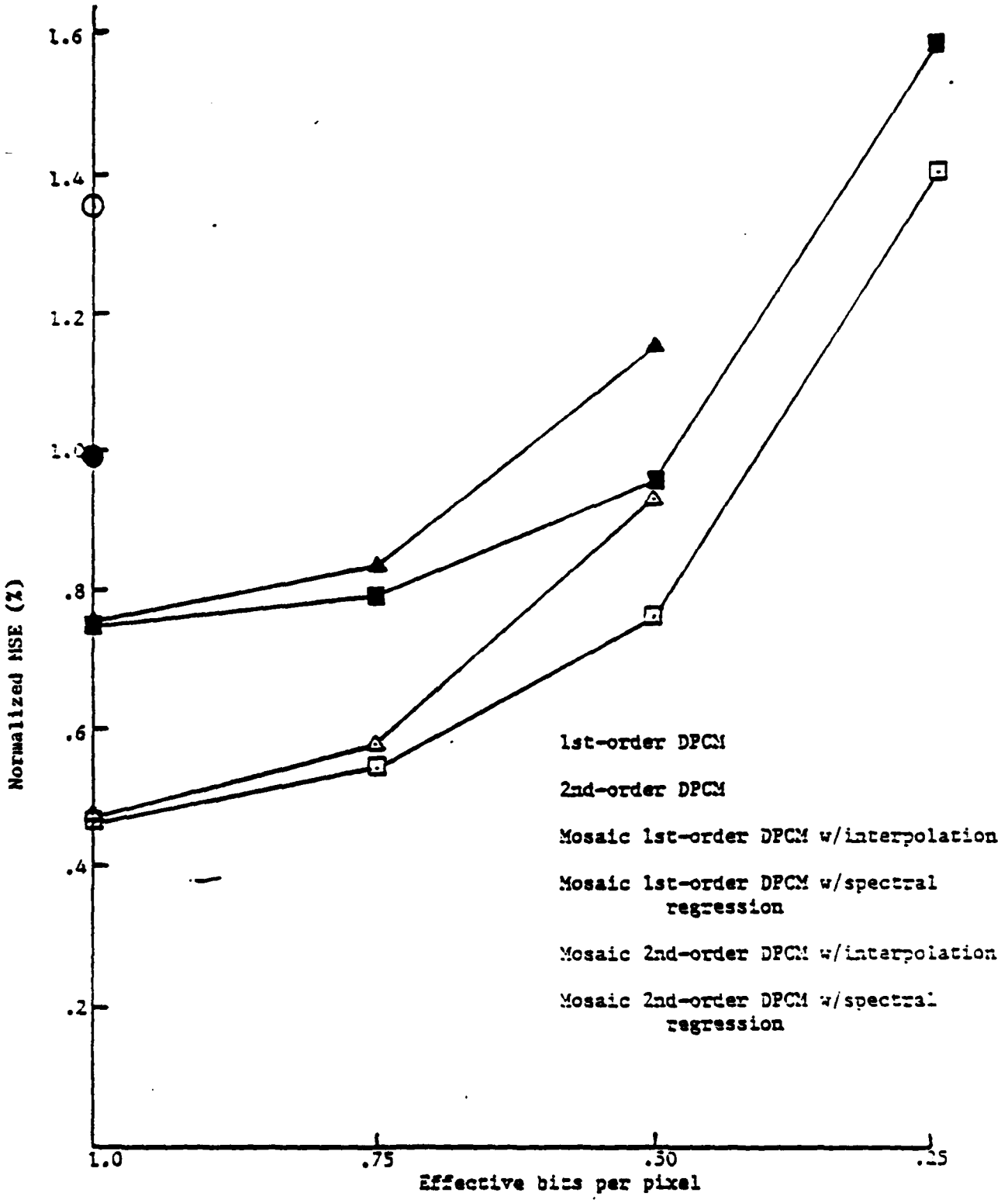

Figure 4. DPCM with spectral regression: NMSE vs bit rate - Band 2

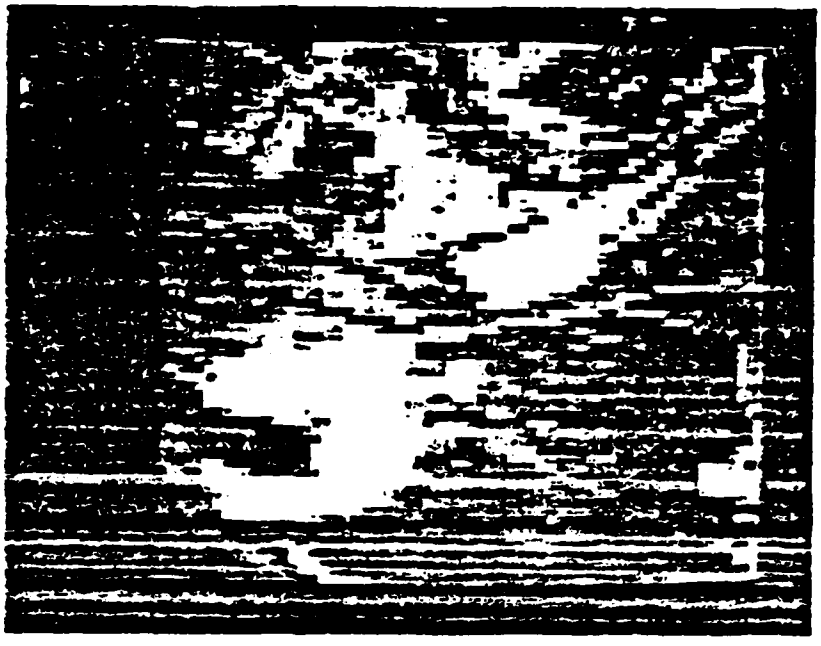

Figure5. Detail of Test Scene, Band 2

Figure 6. One-Band Spectral Regression

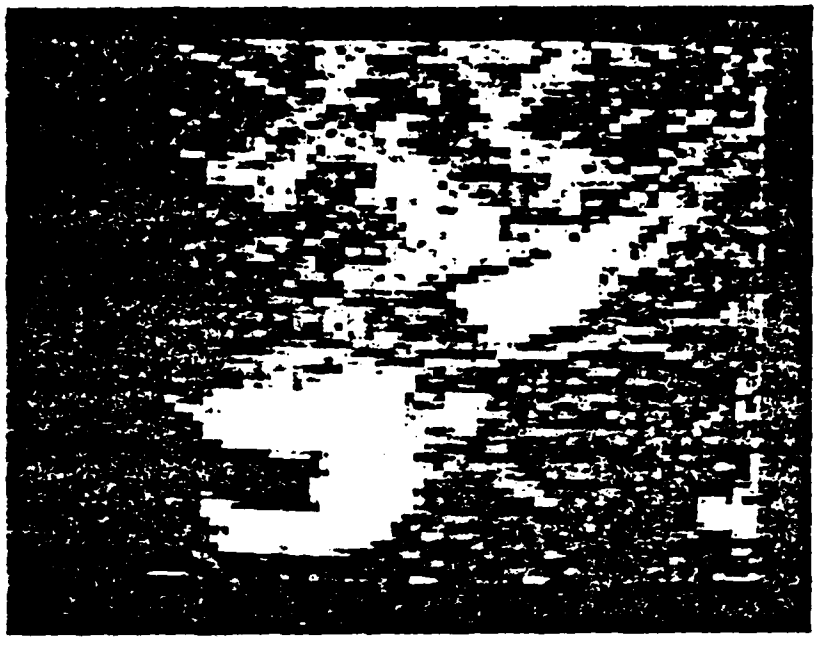

Figure 7. DPCM, 2 bits/pixel

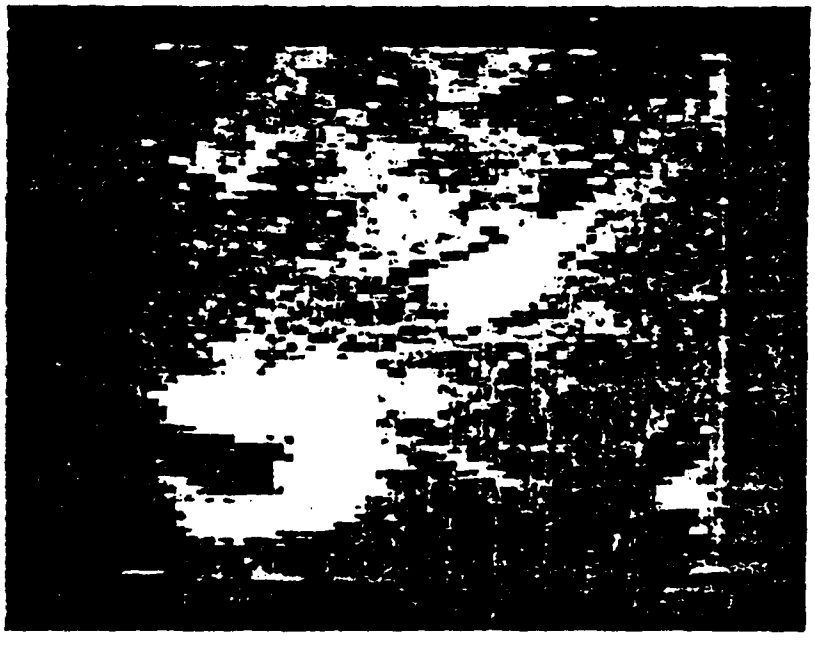

Figure 8. Mosaic DPCM with spectral regression, 0.5 bits/pixel

Optical Implementation

The staggered sampling scheme may be implemented either by a single mosaic focal plane detector array or by a set of staggered linear arrays onto which the scene is scanned by mirrors. Further, the elements may either be of dissimilar construction and spectral sensitivity, or may consist of identical wide-band detectors to which are bonded color filter arrays (CFAs). Solid-state color (RGB) cameras have been constructed which use a set of adjoining linear CCDs, each array being sensitive to only one spectral band. The arrays are deployed in alternating color sensitivity, with elements of each strip offset from the elements of neighboring strips [1]. Alternatively, dye-deposition CFAs have been bonded to sensor chips [2,3,4]. The CFAs are rectilinear masks with repeating pattern $\begin{matrix} R & G \\ G & B \end{matrix}$ [2]; the mask is thus staggered by spectral element but without sensor gaps as was the case in [1]. Configurations up to 484x384 elements with 34 um x 20 um element size have been reported [4]. However, little attempt has been made to estimate imagery in unsampled bands from data in a sampled band; in [3], edge information in the high resolution G band was added directly to the low resolution R and B bands.

References

1. S. Ochi, S. Yamanaka, Y. Kanoh, and T. Nishimura. "A Device Structure and Spatial Spectrum Spectrum for Checker-Pattern CCD Color Camera", IEEE Trans. Electron Devices , Vol. ED-25, pp. 261-266, 1978.

2. B. Bayer, "Color Imaging Array," U. S. Patent 3971065 (1976).

3. P. Dillon, D. Lewis, and F. Kaspar. "Color Imaging System Using a Single CCD Area Array," IEEE Trans. Electron Devices, Vol. ED-25, pp. 102-107, 1978.

4. N. Koike, I. Takemoto, R. Satoh, S. Hanamura, S. Nagahara, and M. Kubo, "MOS Area Sensor: Part I Design Consideration and Performance of an n-p-n Structure 484 x 384 Element Color MOS Imager," IEEE Trans. Electron Devices, Vol. ED-27, pp. 1676-1681, 1980.

(IV.) Tomography in Image Data Compression

Tomography is a technique in which a two-dimensional image may be specified by a number of one-dimensional projections of the image made at different angles. A projection is obtained by integrating the data in one direction across the image, analogous to sweeping a two-dimensional dust pattern on a floor into a line with a wide broom. The original image, or an approximation to it, may be reconstructed from its projections in a number of ways. The most obvious way is to "back-project" the data in each projection across the image plane at the angle of the original projection (the broom analogy in reverse - sweeping the dust line back over a "sticky" floor), producing two-dimensional linear "smears" which are summed to form a two-dimensional image.

A study of image data compression through tomography is being undertaken. This project was proposed to digitally simulate a possible optical implementation, in which projections of a real image are obtained with a rotating, cylindrical lens. The additional observation is that projections are generally slowly varying from one to the next, suggesting that such inherent data redundancy should allow further data compression.

Basic Concepts

It is well known that the one-dimensional Fourier transform of a tomographic projection of an image corresponds to the function along a radial "slice" through the two-dimensional Fourier transform of the image [1]. This allows another method of

image reconstruction, in Fourier space, and gives additional insight into the working of tomography. A short proof of this "correspondence" theorem follows.

Along the horizontal axis, a projection is defined by the equation:

$$f_\theta(y) = \int_{-\infty}^{\infty} f(x,y)dx \qquad (1)$$

where $f(x,y)$ is a two-dimensional image function in x and y, $f_\theta(y)$ is one of its projections at angle θ with $\theta=0$ in this case.

The one-dimensional Fourier transform of (1) is:

$$f_\theta(v) = \int_{-\infty}^{\infty} f_\theta(y).\exp(-2\pi i\ yv)dy \qquad (2)$$

where exp is the exponential function, i is $\sqrt{-1}$ and again with the angle subscript $\theta=0$ in this case.

On the other hand, the two-dimensional Fourier transform of the image function is:

$$F(u,v) = \int_{-\infty}^{\infty}\int_{-\infty}^{\infty} f(x,y).\exp(-2\pi i\ (xu + yv))\ dxdy. \qquad (3)$$

Comparing (2) and (3), it is obvious that:

$$F_\theta(v) = F(u,v)$$

for $\theta=0$, that is $u=0$, proving the theorem in this case.

If new axes are chosen x', y' in the image plane and u', v' in the Fourier plane, each set rotated through an angle θ from the original set, the rotation matrix (old to new) is given by:

$$\begin{bmatrix} \cos\theta & \sin\theta \\ -\sin\theta & \cos\theta \end{bmatrix}$$

which results in the equality of the new and old kernels of the integral in (3), thus:

$$x'u' + y'v' = xu + yv,$$

We have that

$$P_\theta(R) = F(R\cos\theta, R\sin\theta)$$

as an alternate description of the projection slice theorem.

The reconsturction of an image from its set of projections is relatively simple, but requires a careful treatment mathematically. This method we now derive in the following paragraphs, since it is important for the purposes of the computer simulations which we will be carrying out.

Projection Geometries in Data Compression

Using the correspondence theorem we can simulate tomograpny digitally by applying radial filters to a two-dimensional (discrete) Fourier transform of an image. A digital image, held as a rectangular array of data (in x,y) is Fourier transformed, using a two-dimensional, fast Fourier transform (FFT) algorithm. The result is a rectangular array (in u,v). A simple, radial filter is used to zero all data not on the desired, radial lines. An inverse two-dimensional FFT results in an image which has been effectively reconstructed from the corresponding tomogtaphic projections. (See Figure 1 for filter properties.)

By varying the number of radial "slices" in the filter the effect of varying the number of projections on image quality can be observed. A result of the radial nature of the slices is that image low frequencies are well represented, after redundandtly, due to the finite "thickness" (one pixel) of a quantized slice. In contrast, image high frequencies may have

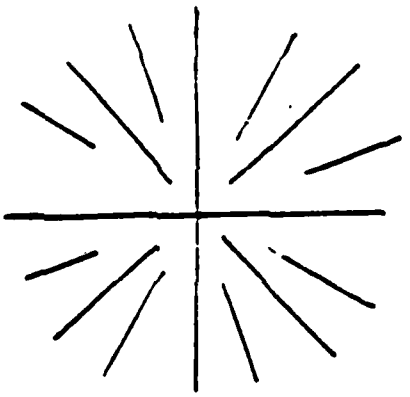

Figure 1. Possible non-redundant, radial filter pattern.

large regions in Fourier space deleted, between the filter slices. The redundancy at low frequencies corresponds to the redundancy previously noted by Hunt that projections are generally slowly varying from one to the next. This can be restated by saying that the higher frequency components of the projections change more rapidly than the lower frequencies as one changes the angle of projection. Thus, the second important procedure is to vary the frequency content of (at least some of) the projections.

Based on $P_\theta(R) = F(R\cos\theta, R\sin\theta)$, we derive the convolution-back-projection method. Consider the inverse Fourier transform of F(U,V) in polar coordinates. The polar coordinates we will use are expressed by

$$\begin{aligned} x &= r\cos\phi \quad , \; r = \sqrt{x^2 + y^2} \qquad 0 \le r \le \infty \\ y &= r\sin\phi \qquad \tan\phi = \frac{y}{x} \qquad 0 \le \phi \le 2\pi \end{aligned} \tag{4}$$

and

$$\begin{aligned} U &= R\cos\theta \quad , \; R = (\sqrt{U^2 + V^2})\,\mathrm{sgn}V, \quad -\infty < R < \infty \\ V &= R\sin\theta \qquad = \tan^{-1}(V/U) \bmod \pi \qquad 0 \le \theta < \pi \end{aligned} \tag{5}$$

so the differential area $dUdV = |R|dRd\theta$.

From these definitions, the polar coordinate Fourier transform of projection data can be written as:

$$f(x,y) = f_p(r,\phi) = \int_0^{\pi} d\theta \int_{-\infty}^{\infty} P_\theta(R)|R|\exp[j2\pi R\cos(\theta-\phi)]dR \tag{6}$$

Let $s = r\cos(\theta-\phi)$, and

$$g_\theta(s) = g_\theta(r\cos(\theta-\phi)) = \int_{-\infty}^{\infty} P_\theta(R)|R|\exp[j2\pi Rs] = P_\theta(s)*q(s) \quad (7)$$

where

$P_\vartheta(s) = F^{-1}\{P_\vartheta(R)\}$ is the projection at angle .

$q(s) = F^{-1}\{|R|\}$ ** is the kernal function .

then

$$f(x,y) = f_p(r,\phi) = \int_0^{\pi} g_\vartheta(r\cos(\vartheta-\phi))d\vartheta \quad (3)$$

Eq. (7) is the convolution (or filtering) of projection $p_\theta(s)$. Eq.(8) is the back-projection of Eq. (7) to obtain the reconstructed image $f_p(r,\phi)$.

If we assume the $f_p(r,\phi)$ is bandlimited by a frequency B, then

$$q(s) = F^{-1}\{|R|\} = \int_{-\infty}^{\infty} |R|e^{jRs}dR = \int_{-\infty}^{\infty} |R|e^{j2\pi Rs}dR$$

$$= 2B^2 \operatorname{sinc} 2Bs\pi - B^2 \operatorname{sinc}^2 Bs\pi . \quad (9)$$

Eq. (7) and Eq. (8) constitute the convolution-back-projection reconstruction method.

Digital Simulations

The above equations are for continuous data. For computer simulations digital samples must be used, and new equations must be developed.

Let the given picture be digitized into a grid of N^2 cells. We assume that the intensity of an entire cell is concentrated

at its center as shown in Fig. 1. Then the pixel A(I,J) at location (x,y) has a corresponding polar coordinate (r,ϕ). where

$$x = (I-0.5) - (N/2.0) \quad , \quad y = (J-0.5) - (N/2.0)$$

$$r = \sqrt{x^2+y^2} \quad , \quad \tan\phi = \frac{y}{x} \quad 0 \leq \phi < 2\pi \qquad (10)$$

Let the projection detector be P(ND), which consists of ND small detectors and the length of per small detector is DL. We assume the pixel A(I,J) contributes to two small projection detectors at most. Refer to Fig. 2, A FORTRAN program for obtaining the projection data P(ND) at the projection angle θ is shown as follows:

```
      DIMENSION A(N,N) , P(ND)
      NTRF = ND/2 + 1
      DO 205 I = 1,ND
205   P(I) = 0.0
C***  θ(in radian) is the projection angle.
      PL1 = ABS(cos(θ))
      PL2 = ABS(sin(θ))
      PL = AMX1(PL1,PL2)/DL
      HAPL = PL/2.0
      DO 215 I = 1,N
      DO 215 J = 1,N
```

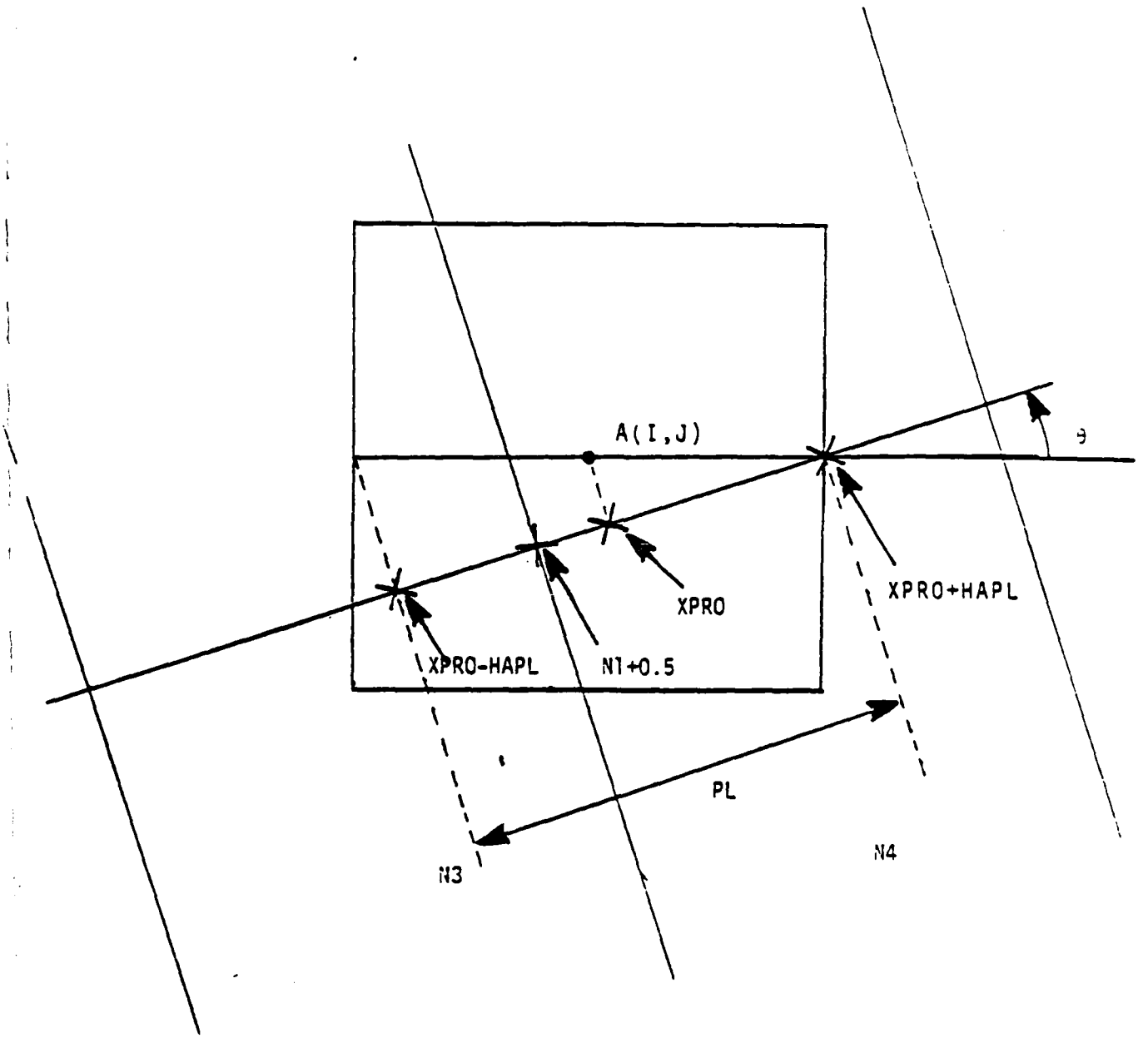

Figure 2. Pixel A(I,J) contributes linearly to two small detectors N3 and N4.

```
      XPRO = (r*cos(§-θ)/DL
C***  (r,§) is the polar coordinate of A(I,J).
      N1 = XPRO-HAPL + 0.5
      IF(XPRO - HAPL .LT. 0.0) N1 = XPRO - HAPL _ 0.5
      N2 = XPRO + HAPL + 0.5
      IF(XPRO + HAPL .LT. 0.0) N1 = XPRO - HAPL - 0.5
      N3 = N1 + NTRF
      N4 = N2 + NTRF
C***  NTRF = ND/2 + 1 to transfer - ND/2≤N1≤ND/2 into 1≤N3≤cND.
      IF(IABS(N4 - N3) . LE.1)GOTO 100
      N5 = N3 + 1
      P(N5) = P(N5) + A(I,J)
      GOTO 215
100   P(N3) = P(N3) + A(I,J)*(N1 + 0.5 - (XPRO -HAPL))/PL
      P(N4) = P(N4) + A(I,J)*(XPRO +HAPL - N1 - 0.5)/PL
C***  A(I,J) contributes linearly to small detectors N3 and N4.
215   CONTINUE
```

Based on the above, we can carry-out the computer implementation of the convolution-back-projection method.

Step 1: For convolution, using Eq. (7),

$$g_\theta(s) = p_\vartheta(s) * q(s) = \int_{-\infty}^{\infty} p_\vartheta(s')q(s-s')ds' \qquad (7)$$

Use discrete convolution

$$g(na,m\Delta) = a \sum_{n'=-\infty}^{\infty} p(n'a,m\Delta)q[(n-n')a]$$

$$g\tilde{}(na,m\Delta) = a \sum_{n'=-ND/2}^{ND/2} p(n'a,m\Delta)q\tilde{}[(n-n')a] \qquad (11)$$

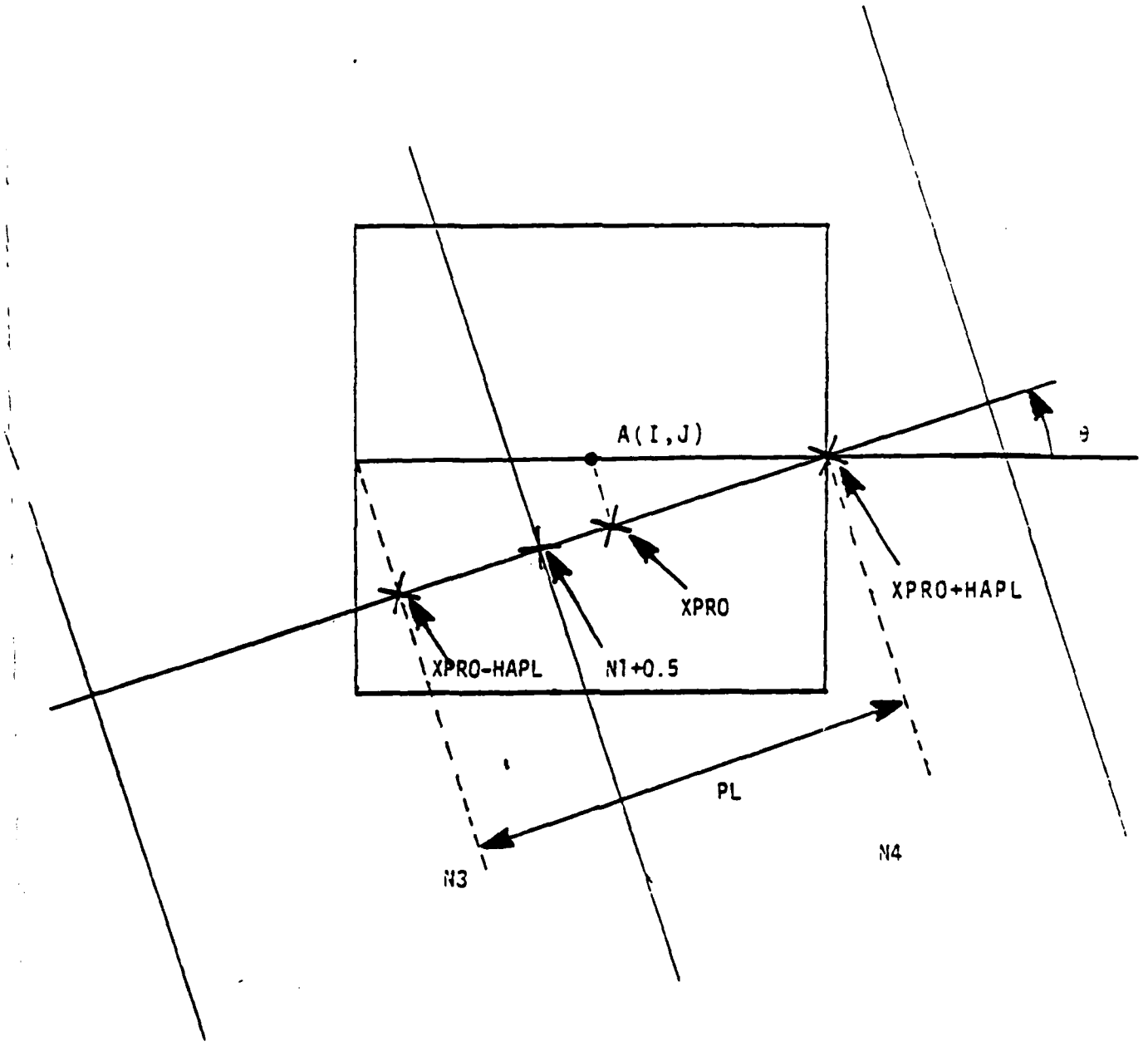

Figure 2. Pixel A(I,J) contributes linearly to two small detectors N3 and N4.

where

$\Delta = \frac{\pi}{M}$, $0 \leq m \leq M-1$ M = the number of projections

$a = DL$ is the length of per small detector.

$-ND/2 \leq n \leq ND/2$, $-ND/2 \leq n' \leq ND/2$

$p(n'a, m\Delta)$ is the projection data at view angle $\theta = \tau\Delta$.

$q(ea)$ is derived from Eq. (9)

$$q(s) = 2B^2 \operatorname{sinc} 2BSTV - B^2 \operatorname{sinc}^2 BS\pi \qquad (9)$$

by letting $s = \ell a$, ℓ: integer, $B = \frac{1}{2a}$ (Nyquist freq.)

$$q(\ell a) = \begin{cases} \frac{1}{4a^2} & \text{for } \ell = 0 \\ -\frac{1}{2_a{}^2 \ell^2} & \text{for } \ell = \text{odd} \\ 0 & \text{for } \ell = \text{even.} \end{cases} \qquad (12)$$

Step 2: For back-projection, using Eq. (8),

$$f(x,y) = f_p(r,\phi) = \int_0^{\pi} g_\theta(r \cos(\theta-\phi))d\theta \qquad (8)$$

Using discrete integral, Eq. (8) can be written:

$$A|(I,j) = f(x,y) = f_p(r,\phi) = \sum_{m=0}^{M-1} g[r \cos(m\Delta-\phi), m\Delta] \quad (13)$$

where

$x = (I-0.5) - N/2.0$, $y = (J-0.5) - N/2.0$.

$y = \sqrt{x^2 + y^2}$, $\tan\phi = \frac{y}{x}$ $0 \leq \phi \leq 2\pi$

Eq. (13) involves interpolation for estimating $g[r\cos(m\Delta-\phi), m\Delta]$ from values of Eq. (11) $g(na, m\Delta)$.

If $na \leq r\cos(m\Delta-\phi) < (n+1)a$,

we estimate $g[r\cos(m\Delta-\phi), m\Delta]$ by

$$g[r\cos(m\Delta-\phi), m\Delta] = \frac{(n+1)a - y\cos(m\Delta-\phi)}{a}\, g(na, m\Delta) + \frac{r\cos(m\Delta-\phi) - na}{a}\, g[(n+1)a, m\Delta].$$

Step 3: Using Eq. (11), Eq. (12), Eq. (13), the computer algorithm operates as follows:

(1) $A1(I,J) = f_p(r,\phi) = 0. \quad 1 \leq I, J \leq N$

(2) Use Eq. (11), (12) to calculate $g(na, m\Delta)$

(3) $A|(I,J) = A|(I,J) + \Delta . g(r\cos(m\Delta-\phi), m\Delta)$

where $= \frac{\pi}{M}$, $0 \leq m \leq M-1$,

repeat steps (2) and (3) M times, then the final reconstructed image $A|(I,J)$ is obtained.

Progress to Date

Some qualitative results have been obtained with a 256x256 element image of a "baboon". This is quite a good test image for the purpose, as it happens to have a significantly flat spatial frequency spectrum due to the fine detail in the baboon's fur, and includes areas of smooth grey values in the eyes and nose. The simple, radial filter has been applied to this image, varying the number of radial slices and the frequency cut-offs of the slice. Surprisingly, the image is still just recognizable with only four filter slices or projection planes. For a

good, qualitative result it seems to be necessary to include a fairly large, central or low frequency region, with a large number of high frequency "rays", forming a filter pattern in Fourier space like a two-dimensional porcupine.

It is intended to continue the experiment in a more quantitative way, comparing image quality both visually and by a measure such as image difference mean squares. In addition, some artificial test-pattern images will be generated, in order to test specific problems with the method.

Also, more complicated radial filters will be tested. For example, if a projection is obtained by integrating also in a circular direction (eg. by "exposing" the projection sensors while the projection angle is being changed), some of the high frequency information lost between the radial filter slices will be utilized (as averaged data). In the simulation, the value at a point on a radial slice in the Fourier domain would be replaced by the average of values lying on a short arc subtended by the (small) angle of integrated rotation. If all values outside the slices are then zeroed as before, the reconstruction is equivalent to rotation of the original image through a (small) angle during each projection "exposure". If, on the other hand, values outside the slices in Fourier space are replaced by the circular averages, the reconstruction is equivalent ot a rotation during summation while constructing an image by back-projection.

Finally, instead of averaging in a circular direction, a maximizing function might be used, thus accentuating (though

in a slightly incorrect position in Fourier space) any dominent frequency component which happens not to fall on a slice.

Simulation Results:

Based on the above algorithm for convolution-back projection, the results for simulating compression are shown in Fig.3, 4, and Table 1.

Method \ M	30	60	100	200
METH = 1**	1.594%	0.545%	0.404%	0.345%
METH = 2***	1.419%	0.553%	0.457%	0.415%

Table 1. NMSE * for different projections numbers M and different kernel functions.

*: NMSE = the normalized mean-square-error. [Ref. 1]

$$NMSE = \frac{\sum_{x,y} [f_r(x,y) - f(x,y)]^2}{\sum_{x,y} f(x,y)^2}$$

**: For method 1, the kernel function q(ea) is

$$q(ea) = \begin{cases} \frac{1}{4a^2} & \text{for } e = 0 \\ -\frac{1}{N^2 a^2 e^2} & \text{for } e = \text{off} \\ 0 & \text{for } e = \text{even} \end{cases}$$

[Ref. 2]

***: For method 2, the kernel function q(ea) is

$$q(ea) = \frac{-2}{\overline{N}^2 a^2 (4e^2 - 1)} \quad , \; l = 0, \pm 1, \pm 2, \ldots$$

[Ref.3]

Figure 3. The reconstructed images of different projection numbers using back-projection method 1.

Figure 4. The reconstructed images of different projection numbers using back-projection method 2.

Optical Implementations

One of the most appealing aspects of the optical compression scheme is how simply it can be implemented. A one-dimensional (cylindrical) lens performs an integration of a scene into a projection. The image being projected can be rotated by any of several simple optical components, such as a Dove prism. The image projections can be formed onto a line detector, such as a CCD array. Thus, very simple and inexpensive hardware is adequate for the optical computation of the image projections.

Equally simple hardware can be used for the reconstruction of the image. This has not been noted before, but is a point which we now discuss*. First, we note from the above discussions that it is necessary first to filter each projection before back-projection. This being done, the back-projection is obviously achieved by a cylindrical lens, where in this case the lens is projecting a line display of the filtered projection into a viewing space. The line display can be made by any of several methods, e.g., a line array of L.E.D.'s or laser diodes. Probably the simplest is a line of intensity written onto the face of a CRT. The rotation of this display at different angles is carried-out as before, e.g., an image rotator prism. If the projections and rotations are carried out at a rate greater than the visual persistence time of the human retina, then a

* The optical reconsturction is due to Donald Fraser, who received support from Grant no. AFOSR-81-0170, while on leave from CSIRO, Australia.

real-time display will be created. Since the original tomographic compression system will be operable at video rates, the reconstruction system will be operable at video rates as well. A simple video-rate optical processing system for data compression can be configured with existing off-the-shelf hardware.

References

1. B. R. Hunt, "Optical computing for image bandwidth compression: analysis and simulation, Applied Optics, Vol. 17, No. 18, pp. 2944-2951, 1978.

2. G. N. Ramachandra and A. V. Lakshminasayanan, "Three dimensional reconstruction from radiographic and electron micrographic application of convolutions instead of Fourier transforms," Proc. Nat. Acad. Sci. U. S., Vol. 68, pp. 2236-2240, 1971.

3. L. A. Shepp and B. F. Logan, "The Fourier reconstruction of a head section," IEEE Trans. Nucl. Sci., Vol. NS-21, pp. 21-42, 1974.

(V.) Applications of Stationary Transform Processing

We report here two image processing applications of stationary transform processing [1], (also described in the 1981-82 Annual AFOSR Report). The areas of concern are image data compression, and image restoration. In both areas, using the stationary radiometric and geometric transforms in conjunction with nonadaptive processing algorithms proves to be superior to the application of nonadaptive processing alone. In section (V.1) we show results of data compression which achieve 0.6 bits/pixel for good quality imagery. Also, a scheme for hybrid optical/digital implementation is proposed. Finally in section (V.2), we briefly describe some new work in which we are investigating the application of stationary processing to spatially-variant image restoration.

(V.1) Data Compression

The success of image data compression methods is closely linked to the statistical behavior of the data. Conventional nonadaptive predictive coding employs a global predictor to describe the spatial correlation of the image. However, realistic imagery rarely exhibits stationary statistical properties. Consequently, the nonadaptive approaches to predictive, transform, and hybrid coding are far from optimum. Superior performance is characteristic of the more sophisticated adaptive image coding techniques [2]. An example is adaptive DPCM, which

is a form of predictive coding where the coefficients of the optimum predictor are tuned to the local image statistics. This adaptation to statistical behavior leads to increased data compression for given image quality, or increased image quality for the equivalent bit rates of nonadaptive DPCM. Similar benefits of adaptive methods are found in transform coding and hybrid coding.

We consider here the reverse approach to the adaptive coding problem. Starting with a nonstationary image, we propose to use a radiometric/geometric transform [1] which generates an image with approximately wide-sense stationary first and second moment statistics. Due to this stationarity, the transformed image is matched to nonadaptive coding processes. After coding and transmission of the transformed image data plus certain transform coefficients, the received image is reverse transformed.

Stationary transform processing incorporates two separate stages: a radiometric transform which generates nearly stationary mean and variance; followed by a geometric transform, or warp, to give approximately stationary autocorrelation width. In general, it will be seen that coding using stationary transforms bears certain similarities to both predictive and transform coding. We show that the radiometric transform acts in a somewhat similar fashion to the adaptive quantizers found in other adaptive coding methods. The geometric transform is shown to be a flexible and convenient means for implementing variable spatial resolution for reducing spatial redundancy within scenes. We consider in particular stationary transforms

applied to IDPCM (interpolative DPCM) data compression [3]. IDPCM is a coding technique which incorporates the essential principles of conventional digital DPCM coding; it has been proposed for implementation using hybrid digital/optical hardware. In this paper, we suggest that stationary transforms are also suitable for hybrid digital/optical configurations.

Applying Radiometric Transforms to Data Compression

PCM coding generally yields images of acceptable quality using a minimum of 5 bits, or 32 gray levels. Use of fewer bits results in "false contouring", especially in low contrast scenes, since relatively large regions may be assigned to a single quantum level. Adaptive quantizers [4], [5] have been developed which adaptively expand low contrast regions into the full dynamic range of the quantizer, thereby reducing the contouring problem. Our scheme for achieving lower bit rates operates along similar lines. The data compression scheme is outlined in Fig. 1.

The reduction in contouring effects using the radiometric transform permits us to use lower bit rates. As Fig. 1 indicates, we also need to transmit the values of μ_N and K for each sub-block. The total bits can be calculated from the equation

$$B_{total} = N^2 n + 16 \left[\frac{N}{M}\right]^2 \qquad (1)$$

where the original image is of size N by N, n is th number of bits used in quantizing the transformed data, and M is the

sub-block size. The factor of 16 is due to the two bytes used to code μ_N and K per sub-block. The number of bits/pixel is

$$B/\text{pixel} = n + \frac{16}{M^2} \qquad (2)$$

From Eq. (2), the overhead bit rate needed to transmit the transform coefficients is $16/M^2$; sub-blocks of 8 by 8 pixels require 0.25 bits/pixel, for example. Larger sub-blocks of 16 by 16 pixels require only 0.063 bits/pixel; however, the image quality is slightly inferior.

Figures 2(a)-(f) illustrate several stages of the compression scheme in Fig. 1. False contouring is exhibited in Fig. 2(b), which represents normal 3 bit PCM coding. To overcome this distortion, mean and variance statistics are measured in contiguous sub-blocks of 8 by 8 pixels in the "Walter" image of Fig. 2(a); these values are then used in the radiometric transform [1] in blockwise fashion to generate Fig. 2(c). The stationary value $\sigma_s = 100$ is sufficient to adaptively expand the dynamic range of each sub-block to fill the available 8 bit range. In Fig. 2(d), uniform 8 level quantization has been performed at levels 16, 48, 80,...,240. The inverse transform [1] yields Fig. 2(e). From Eq. 2 the final bit rate is 3.25 bits/pixel. Figure 2(f) is the end result of similar processing, except we have used only 4 quantization levels after transformation. The bit rate is 2.25 bits/pixel. Quantization distortion and a block structure become apparent at this bit rate. Data compression by the radiometric transform method bears some resemblance to the method of block truncation coding [6].

Both techniques require measurement of block statistics, followed by a quantization scheme based on these statistics.

Applying Geometric Transforms to Data Compression

In [1] we discussed a geometric transform or warp which generates approximately stationary autocorrelation length in contiguous sub-blocks of an image. This was achieved by locally expanding (by nonuniform interpolation) sub-blocks of low correlation, for example, edges. Consider now an alternative way of generating near-stationarity correlation: compress or shrink regions of high correlation until they possess the same correlation factor as, say, the least correlated neighborhood. Following the procedure outlined in [1], we select $\rho_{s(NS)}$ and $\rho_{s(EW)}$ to be the maximum value of ρ in NS and EW directions, respectively, over all sub-blocks; and apply compression vactors, F, to each sub-block, determined by

$$F_{NS} = \frac{\rho_{NS}}{\rho_{s(NS)}} \; ; \; (0 < F_{NS} \leq 1), \qquad (3)$$

with a similar equation for F_{EW}.

The algorithm in [1] is used to compute warp control points from the F_{NS}, F_{EW} values. A scheme for data compression via geometric transformation is shown in Fig. 3. This process affords a method of varying the spatial sampling interval, or resolution, in order to compensate for high correlation or spatial redundancy.

Each sub-block of the radiometric transform data-compressed image (Fig. 2(e)) is represented in the geometric transform by

the following number of pixels,

$$B/\text{sub-block} = M^2 F_{NS} F_{EW} \tag{4}$$

The total pixels for an image of size N by N is

$$B_{total} = M^2 \sum_{\text{all } N} F_{NS} F_{EW} \tag{5}$$

Assuming that a pair of bytes is sufficient to represent a pair of control points, the number of overhead bits is

$$B_{\text{control points}} = 16 \left(\frac{N}{M} + 1\right)^2 \tag{6}$$

Ignoring the factor of 1 in Eq. (6), the final bit rate using radiometric and geometric transforms is, from Eqs. (2), (5) and (6),

$$B/\text{pixel} = \underbrace{n \frac{M^2}{N^2} \sum_{\text{all } N} \left[F_{NS} F_{EW}\right]}_{\text{image data}} + \underbrace{\frac{32}{M^2}}_{\text{overhead}} \tag{7}$$

The bit rate calculation above assumes equal-sized sub-blocks in the computation of the two transforms. In practice, we can usually use larger, hence fewer, blocks for the geometric transform with little effect on image quality. Block dimension is more critical to image quality in the radiometric transform. Substituting new sub-block sizes M_R and M_G in Eq. (7) gives

$$B/\text{pixel} = n \frac{M_G^2}{N^2} \sum_{\text{all } N} F_{NS} F_{EW} + 16 \left[\frac{1}{M_G^2} + \frac{1}{M_R^2}\right] \tag{8}$$

ie. if $M_R = M_G$, Eq. (8) reduces to Eq. (7)

Following the procedure in [1], we measure the values of ρ_{NS} and ρ_{EW} at each sub-block, and, from Eq. (3), compute the compression ratios F_{NS} and F_{EW}. In accordance with the threshold limitations on ρ_{NS} and ρ_{EW}, the ranges of F_{NS} and F_{EW} are 3:1 and 2.6:1, respectively. Applying the geometrical transform based on F_{NS} and F_{EW} [1], we obtain the warped version of Fig. 2(e) in Fig. 4(a). Notice that regions of low correlation remain relatively unwarped, compared with regions of high correlation which have been undersampled (along and axis) by a factor approaching 3:1. The inverse warp produces Fig. 4(b).

The terms in Eq. (8) are: $n = 3$, $N = 256$, $M_G = 16$, $M_R = 3$, and $\Sigma F_{NS}F_{EW} = 105$. The final bit rate of Fig. 4(b) is therefore 1.2 bits/pixel.

Applying Stationary Transforms to IDPCM Data Compression

Interpolative Differential PCM (IDPCM) was originally conceived [3] as a vehicle for implementing conventional DPCM using hybrid digital/optical hardware. The method involves dividing the image into low and high frequency components, then taking advantage of the statisitcal properties of each component to achieve data compression. Specifically, the low frequency image is highly correlated, consequently only every other pixel on every other line is transmitted, using 5 bits/pixel (to avoid false contouring). The high frequency component has a small absolute range of amplitudes, and low correlation, hence every pixel is transmitted, except at locations where the low frequency data is transmitted. However, it has been shown [7]

that a binary, or 1 bit, representation is sufficient to preserve subtle edge details when added back to the low frequency component. The bit rate is computed using

$$\text{B/pixel (IDPCM)} = \frac{1}{4}\,\text{LF} + \frac{3}{4}\,\text{HF} \qquad (9)$$

where LF and HF are the bits/pixel used in the low and high frequency image components, respectively. Hence, using LF = 5 and HF = 1, good quality imagery can be realized with a data rate of 2 bits/pixel.

IDPCM has two areas for potential improvement of bit rates:

(1) The 5 bit coding of the low frequency image is inefficient.

(2) Except for the subsampling of the low frequency image, no attempt is made to compensate for spatial redundancy (high correlation).

We address these areas using the radiometric and geometric transforms, respectively. Figure 5(a) illustrates our proposed inclusion of stationary transforms in IDPCM. The geometric transform is first applied to reduce the spatial redundancy between correlated pixels in the original image. We then apply the radiometric transform to "adaptively quantize" the low frequency component. Fig. 5(b) shows the reconstruction operation.

In computing the final bit rate, we need to consider four separate contributions:

(i) low frequency image: $\left[\frac{N^2}{4}\right]\left[LF\right]\left[\frac{M_G^2}{N^2}\right]\left[\sum_{\text{all } N} F_{NS}F_{EW}\right]$ bits

(ii) high frequency image: $\left[\frac{3N^2}{4}\right]\left[HF\right]\left[\frac{M_G^2}{N^2}\right]\left[\sum_{\text{all } N} F_{NS}F_{EW}\right]$ bits

(iii) radiometric transform overhead: $\frac{16\ N^2}{M_R^2}$ bits

(iv) control points overhead: $16\left[\frac{N}{M_G}+1\right]^2 \approx 16\ \frac{N^2}{M_G^2}$ bits

Summing (i) - (iv) and dividing by N^2 gives the final bit rate:

$$\text{B/pixel (enhanced IDPCM)} = \left[\frac{LF}{4}+\frac{3}{4}HF\right]\left[\frac{M_G^2}{N^2}\right]\left[\sum_{\text{all } N} F_{NS}F_{EW}\right] + 16\left[\frac{1}{M_R^2}+\frac{1}{M_G^2}\right] \qquad (10)$$

Figures 6(a) and 6(b) are the results of data compression by enhanced IDPCM using sub-blocks of 8 by 8 and 16 by 16 pixels, respectively, for the radiometric transform (the parameter M_R); both use 16 by 16 blocks for deriving the geometric transform (the parameter M_G); Final bit rates are 0.75 and 0.56 bits/pixel, respectively. The few artifacts which appear in Fig. 6(b) are caused by the larger sub-block dimension of the radiometric transform.

Hybrid Optical/Digital Implementation of Enhanced IDPCM

To implement the IDPCM technique described above using radiometric and geometric transforms, the following sequential operations are required:

(A) A linearly subsampled version of the geometrically and radiometrically transformed image is generated, quantized, coded, and transmitted. (Fig. 5(a)). This is the low frequency channel. At the same time, a subsampled version of the geometrically transformed image that is not radiometrically transformed is blurred (i.e., interpolated) to produce the low frequency channel. This blurred image is stored.

(B) The blurred image from the previous step is subtracted from the geometrically transformed original image, producing the geometrically transformed high frequency image. This image is quantized, coded, and transmitted.

(C) Reconstruction: At the receiving end, the sub-sampled image from Step (A) is decoded; then the inverse radiometric transform is applied. (Fig. 5(b)). This subsampled image is then blurred (in identical fashion to the blurring in Step (A)) to generate the geometrically transformed low frequency image. Note that the geometric transform is implicit in the transmitted, subsampled image, and that the subsampling is in the form of a two-dimensional linear array. The blurring is not associated with the geometric transform, but simply fills in the missing pixels between the uniformly sampled points. This low frequency image is added to the decoded high frequency image, and the inverse geometric transform applied to the summed image generates the final image.

In [1] we gave details of hybrid optical/digital hardware for realizing block stationary transforms. We do not include

hybrid data compression architecture here, since the principles are essentially those of reference [1].

(V.2) Image Restoration

We are currently investigating the following problems.

1. Spatially-variant deblurring
2. Spatially-adaptive noise filtering

Nonadaptive noise filtering is hampered by the inherent non-stationarity of image data. For example, the lowpass filter required to achieve the desired reduction in noise power may cause intolerable blurring of edge details. On the other hand, a filter which cuts off at a higher frequency may not produce enough noise smoothing. What is needed, therefore, is a filter which can adjust its cut-off frequency according to local image detail i.e., cut-off being inversely proportional to correlation. We are approaching the problem by using the geometric transform to give images of approximately stationary correlation. Non-adaptive filtering is then performed on the transformed images, followed by inverse transformation. (The radiometric transform is not used in this case, since stationary mean and variance are of no benefit to noise-smoothing.) Stationarity in correlation length ensures that edges are preserved even for high degrees of noise smoothing. A preliminary result of spatially-adaptive filtering is processed in Fig. 7. The improvement gained by adaptive filtering is marred by striations caused by noise correlations inherent in the filtering of geometrically transformed images. We are currently investigating ways of avoiding this effect.

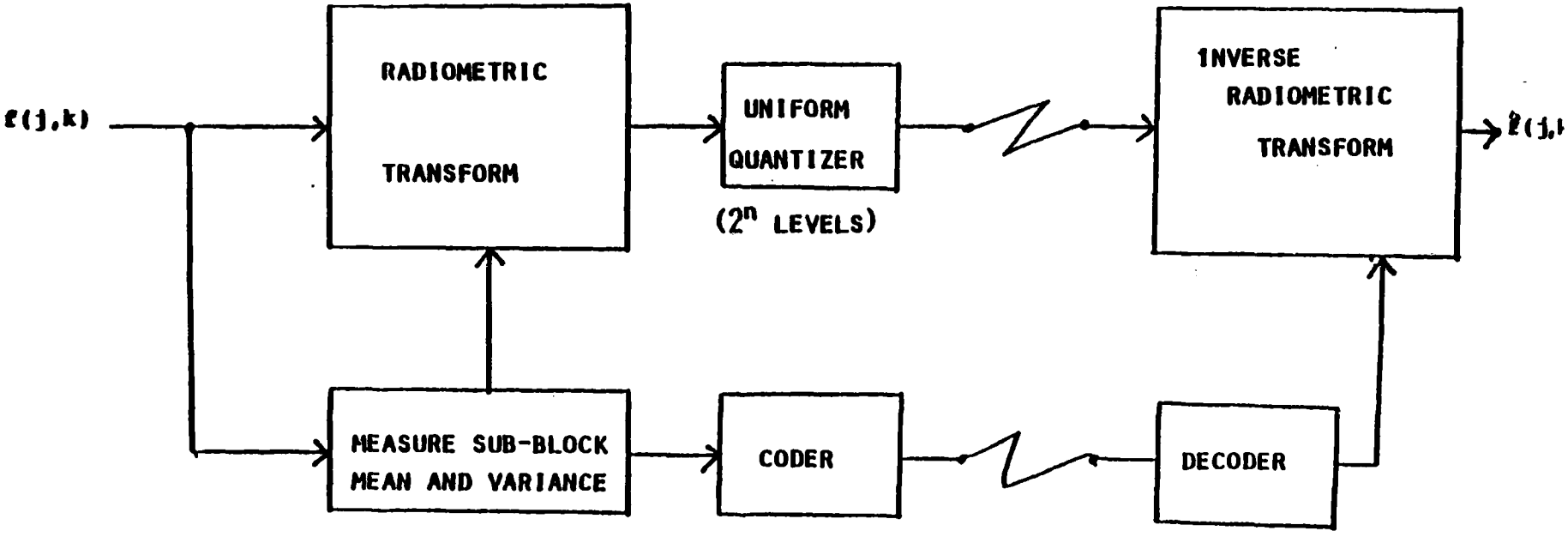

Figure 1. Data Compression by Radiometric Transform.

(a) Original

(b) 3-bit PCM

Fig.2. Example of data compression using the Radiometric Transform.

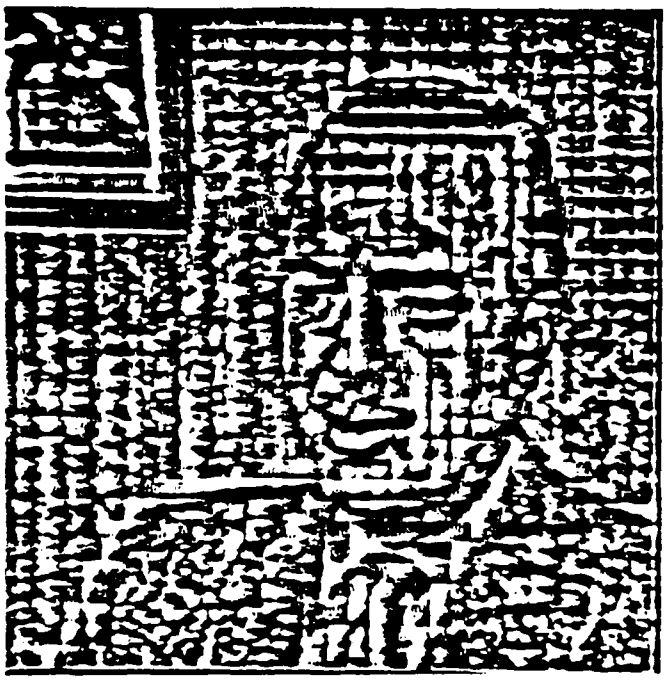

(c) Radiometric Transform

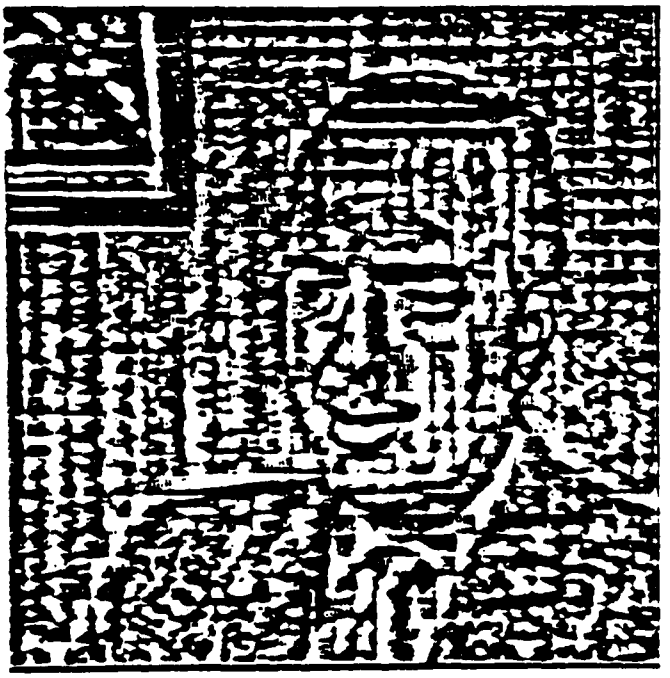

(d) Radiometric Transform after 8 level quantization

Fig. 2 (continued)

(e) Inverse Radiometric Transform (3.25 bits/pixel)

(f) Repeat of 2(d),(e) using 4 levels (2.25 bits/pixel)

Fig. 2 (continued)

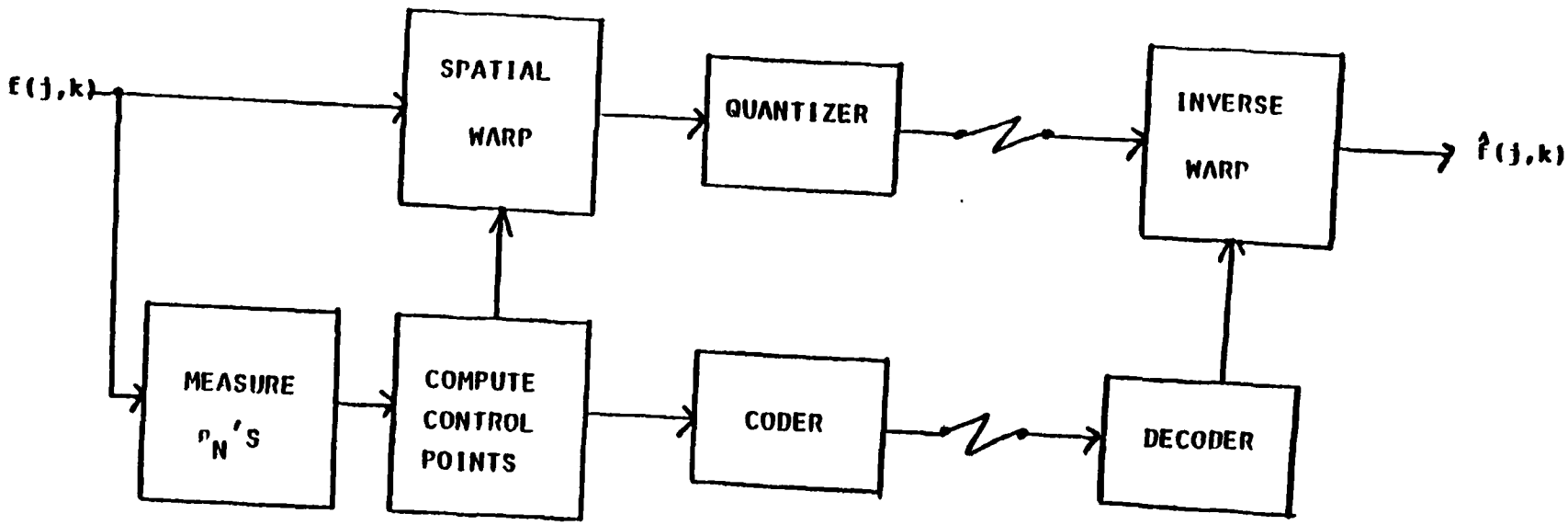

Figure 3: Data Compression by Geometric Transform.

(a) Geometric Transform of Fig. 2(e).

Fig. 4. Example of Data Compression by Radiometric/Geometric Transforms.

(b) Result of data compression using the Radicmetric/Geometric Transforms (1.2 bits/pixel)

Fig.4. (continued)

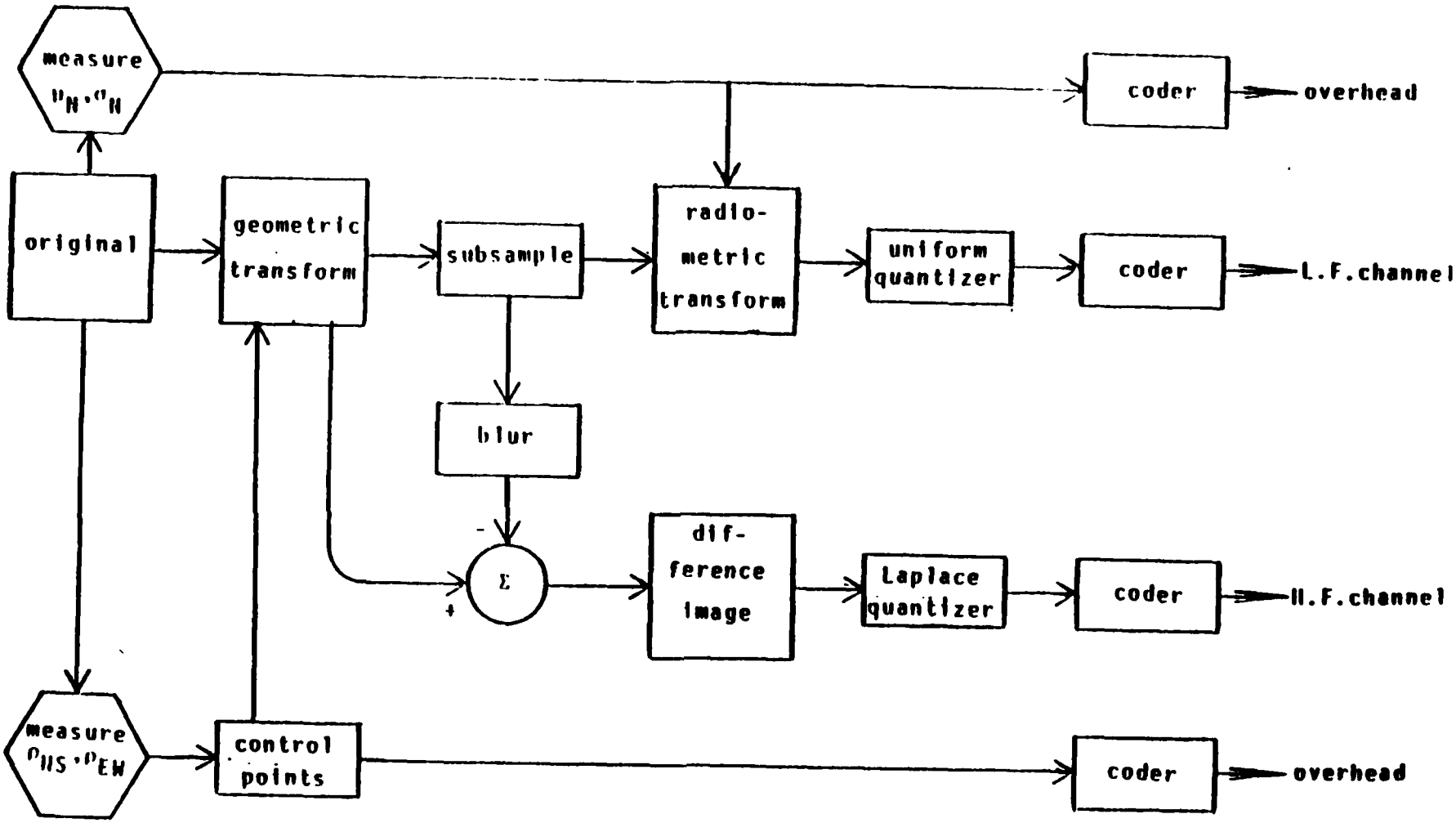

Figure 5(a) Enhanced IDPCM Architecture - Generation of low and high frequency channels.

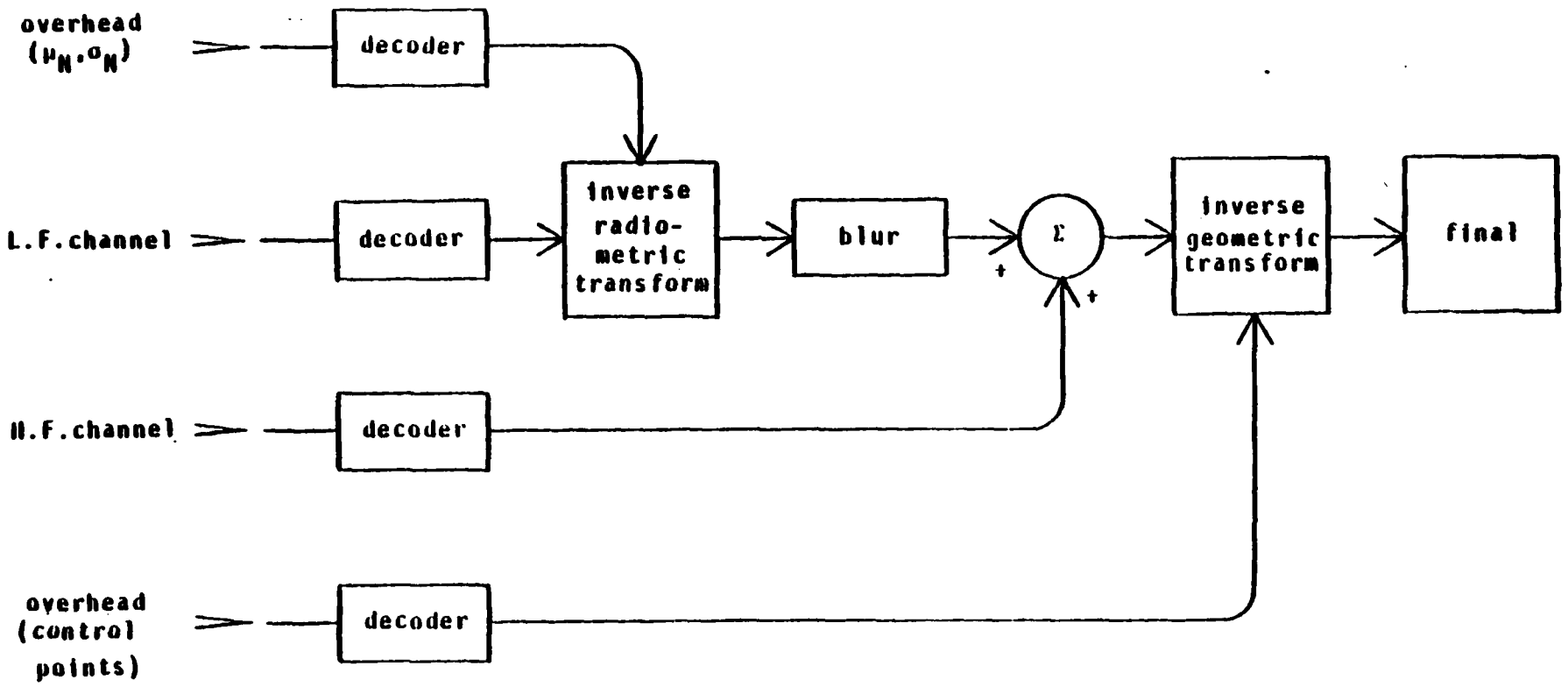

Fig. 5(b) Reconstruction

(a) $M_R = 8$ $M_G = 16$ 0.75 bits/pixel

(b) $M_R = 16$ $M_G = 16$ 0.56 bits/pixel

Fig. 6. Enhanced IDPCM results.

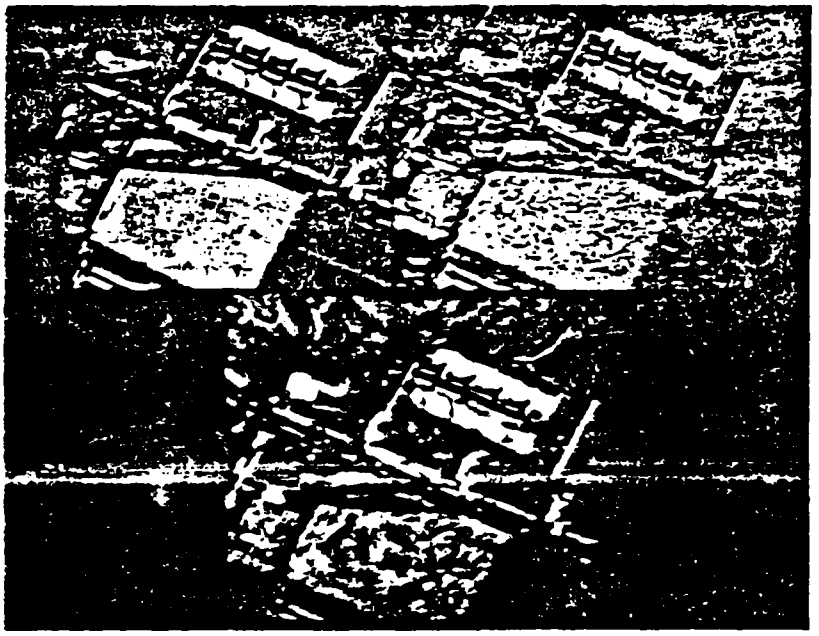

Figure 7. Spatially Adaptive Noise Filtering.
top left - original
top right - original plus noise
center - adaptively-filtered

References

1. R. N. Strickland, Transforming Images into Block Stationary Behavior, accepted for publication in Applied Optics, to be published May 1983.

2. A. Habibi, Survey of Adaptive Image Coding Techniques, IEEE Trans. Comm., COM-25, 1977, pp. 1315-1322.

3. B. R. Hunt, Optical computing for image bandwidth compression: analysis and simulation, Applied Optics, 17, no. 13, 1978. pp. 2944-2951.

4. P. Cummiskey, N. S. Jayant and J. L. Flanagan, Adaptive quantization in differential PCM coding of speech, Bell Syst. Tech. J., 52, pp. 1105-1118.

5. D. J. Goodman and A. Gersho, Theory of an Adaptive Quantizer, IEEE Trans. Comm., COMM-22, 1974, pp. 1073-1045.

6. E. J. Delp and O. R. Mitchell, Image Compression using Block Truncation Coding, IEEE Trans. on Communications, COM-27, no. 9, 1979, pp. 1335-1342.

7. H. N. Ito and B. R. Hunt, Temporally Adaptive Hybrid Optical/Digital Interframe Compression Scheme, Proc. SPIE 292, Processing of Images and Data from Optical Sensors, 1981, pp. 77-85.

(VI.) Improved IDPCM Data Compression

The first technique which was successful in demonstrating an optical architecture for image data compression was the method referred to as IDPCM (Interpolated Differential Pulse Code Modulation). The essence of this method is to split the image into two components: a low-frequency component which is created by optical subsampling and optical interpolation (via incoherent convolution), and a high-frequency component created by subtracting the low-frequency component from the original image. The method can be implemented by simple optical masks, mis-focused apodized lenses, and video subtraction imaging [1].

The data compression performance of IDPCM is adequate but not impressive. Indeed, the overall image quality at a given bit rate is often reminiscent of conventional DPCM data compression. For example, little if any degradation in image quality is seen for images compressed from 8 bits/pixel to 3 bits/pixel by both DPCM and IDPCM. Dropping the bit rate to 2 bits/pixel leads to visible losses in image information for both DPCM and IDPCM. An open question, therefore, is how to achieve better performance from the IDPCM concept. One alternative is the stationarity transformations discussed in the previous section. With these methods image compression rates of less than 1 bit/pixel have been achieved for IDPCM. The stationary transform methods appear to be somewhat complex in system architecture, however, and a desire exists to find improvements to IDPCM which are less complicated.

An avenue of pursuit for improved IDPCM is in the Fourier coding technique which has been used so extensively in digital image data compression. In this method an image is decomposed into blocks and the 2-dimension FFT is computed on each block. The Fourier coefficients produced in each block are then re-quantized. The key to data compression by this method is in the requantization. Typical images show a wide dynamic range in the computed Fourier spectrum, with the largest values occuring near D. C. and the smallest values near the Nyquist frequency. Since the dynamic range is so wide, it is not necessary to carry the same number of bits of significance in quantizing all coefficients of the image FFT. For example, by a suitable pre-assigned mask, which indicates the scale-factor associated with unit increments of quantization at each spatial frequency coefficient, it is possible to quantize coefficients near D. C. at 8-10 bits and coefficients near Nyquist frequency at 0-2 bits, with little overall error. Using these techniques in an adaptive mode, it is possible to create quantization schemes with bit rates on the average of less than 1 bit per pixel.

The applicability of this technique to IDPCM has been the subject of the current set of investigations. There is substantial difference between IDPCM coding of imagery and conventional Fourier coding of imagery, and this difference leads to questions as to the applicability of Fourier coding to IDPCM. Specifically, Fourier coding integrates the low spatial frequency and high spatial frequency components into one set of quantization

assignments for the Fourier frequency components. However, an IDPCM image is split into two parts, a separate low- and high-spatial frequency set of image samples.

Analysis of the IDPCM technique indicates the efficiency with which the low spatial frequency component is represented. For example, consider an image with 8 bits per sample initial data rate. If the subsample rule required for IDPCM [1] is chosen to be every other pixel and line, then the effective rate for representation of low frequencies is 8/4 = 2 bits/pixel. Further, it has been shown that the low frequency subsamples need not be retained at the 8-bits/pixel of the original, and 4 bits per subsample leads to high-quality results at an average rate of 1 bit/pixel. Thus, the low-spatial-frequency component can now be represented in IDPCM with rates of 1 bit/pixel or less [1]. This indicates the area for concentrating upon Fourier coding is the high-frequency component of IDPCM.

Analysis of Fourier coding schemes indicates that the highest spatial frequencies in an image are representable with a very small number of bits. An example can be seen in Pratt's book [2], where a typical bit assignment mask for a Fourier coding algorithm averages less than 1-bit per pixel for the high-frequencies. Indeed, it is aften possible to neglect the highest spatial frequencies in both x and y directions. That is, a typical bit assignment mask may assign one-bit per Fourier coefficient to the x or y Nyquist frequency, but zero-bits to the joint Nyquist frequency of x and y. (See Fig. (VI.1)).

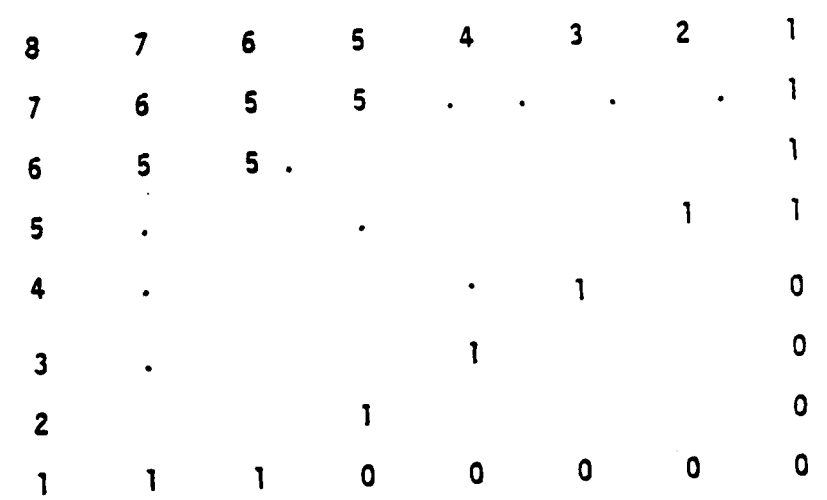

Figure VI.1.

In Figure VI.1 we see the dominance of low frequencies for the assignment of quantization bits. In an IDPCM system, the low frequencies are subtracted out from one image, so that the high frequency components would represent only the values that would require quantization coding. A mask for the Fourier coding of the high-frequency spatial component might appear, for example, as in Figure VI.2:

0	0	0	0	2	1	1	1
0	0	0	0	2	1	1	1
0	0	0	0	2	1	1	1
0	0	0	0	2	1	1	0
2	2	2	2	2	1	0	0
1	1	1	1	1	0	0	0
1	1	1	1	0	0	0	0
1	1	1	0	0	0	0	0

The overall bit-rate for the high-spatial frequencies coded with this bit assignment would be much less than one bit per pixel (i.e., 0.677). Combined with an efficient sub-sampling and re-quantization of the low spatial frequency components, a bit rate of substantially less than 1-bit per pixel should be achievable, with acceptable image quality.

The design of the bit mask for a Fourier coding scheme can not be done by analytic model. The current method for bit mask by trial-and-error studies over a variety of images which are selected to be typical of the class of images to be processed through the data compression system. Thus, additional research on this problem becomes one of simulation, experiment, and visual

verification. Initial results indicate that:

(1) The Fourier coding of IDPCM images should produce images of visual quality equal to that of conventional Fourier coding of images;

(2) The bit-rates associated with a Fourier coding of IDPCM will be competitive with conventional Fourier image coding.

Since IDPCM was an optical method for image data compression, the introduction of Fourier coding leads to a hybrid optical/digital method for image data compression. The reference to a "hybrid" method stems from the fact that the most straignt-forward means to implement the Fourier coding would be by a digital Fourier transform of the high-frequency component of IDPCM.

References

1. B. R. Hunt, "Optical computing for image bandwidth compression: analysis and simulation," Applied Optics, vol. 17, pp. 2944-2951, 1978.

2. W. K. Pratt, Digital Image Processing, Wiley and Sons, New York, 1978.

(VI.) LIST OF PUBLICATIONS RESULTING FROM AFOSR SUPPORT

(1) B. R. Hunt, "Some remaining problems in nonlinear image restoration", Proc. Symp. Image Science Mathematics, Navel Postgrad. School, Monterey, Calif. Nov. 10-12, 1976.

(2) B. R. Hunt, "An optical analogy to DPCM digital image data compression", Proc. SPIE, Vol. 118, August, 1977.

(3) D. G. McCaughey, "An image coding algorithm using spline functions", Proc. SPIE, Vol. 149, August, 1978.

(4) D. G. McCaughey and H. C. Andrews, "Image approximation by variable knot bicubic splines".

(5) B. R. Hunt, "Optical computations for image bandwidth compression: analysis and simulation", Appl. Optics, Vol. 17, pp. 2944-2951, 1978.

(6) D. J. Granrath and B. R. Hunt, "Signal detection trade-off analysis of optical vs. digital Fourier transform computers", Appl. Optics, Vol. 18, pp. 36-43, 1979.

(7) D. J. Granrath and B. R. Hunt, "A two-channel model of image processing in the human retina", Proc. SPIE, Vol. 199, August, 1979.

(8) B. R. Hunt, "Nonstationary statistical image models", Computer Graphics and Image Processing, Vol. 12, pp. 173-186, 1980.

(9) D. G. McCaughey, "Variable resolution hybrid-coding techniques", ASSP Workshop on Two-Dimensional Signal Processing, Berkeley, 1979.

(10) D. G. McCaughey and H. C. Andrews, The continuous-discrete model: least-squares inverses and singular function expansions".

(11) B. R. Hunt and S. D. Cabrera, "Optical implementation of a spatially adaptive image data compression scheme", Proc. SPIE, Vol. 232, Washington, 1980.

(12) B. R. Hunt, and H. Ito, "A hybrid optical/digital interframe image data compression scheme", Proc. SPIE, Vol. 249, San Diego, 1980.

(13) B. R. Hunt and S. D. Cabrera, "Optical computations for a spatially adaptive image data compression system", Optical Engineering, Vol. 20, pp. 616-620, 1981.

(14) H. Ito and B. R. Hunt, "A temporally adaptive hybrid optical/digital interframe compression scheme", Proc. SPIE, Vol. 292, San Diego, 1981.

(15) W. R. Stevens and B. R. Hunt, "Software pipelines in image processing", Computer Graphics and Image Processing, Vol. 20, 1982.

(16) R. N. Strickland, "Adaptive data compression by transformations for generating stationary statistical image models", Proceedings of the York Conference on Image Processing, York, U. K., 1982.

(17) R. N. Strickland, "Transforming images into statistically stationary behavior", accepted for publication, Applied Optics.

(18) W. Smith and R. N. Strickland, "Adaptive data compression by statistically stationary transformations", accepted for publication, Applied Optics.

(19) B. R. Hunt, O. Kubler, "An optimal theory of multispectral image restoration", SPIE Proc. Vol. 397, Geneva, April 1983.

(20) S. Park, R. Schowengerdt, "Image reconstruction by parametric cubic convolution", Computer Graphics and Image Processing, Vol. 20, 1982.

(21) R. Schowengerdt, S. Park, R. Gray, "Topics in the 2-dimensional sampling and reconstruction of images", Int'l Journal of Remote Sensing, March 1983.

(22) S. Park, R. Schowengerdt, "Image sampling, reconstruction, and the effects of sample-scene phasing", Applied Optics, Vol. 21, Sept. 1982.

(VII.) Personnel

The following is a list of personnel who received partial support from Grant AFOSR-81-0170 during the period from March 15, 1982 to March 14, 1983.

Professor B. R. Hunt: Principal Investigator.

Assistant Professor R. N. Strickland: Department of Electrical Engineering.

Assistant Professor R. Schowengerdt: Remote Sensing and Department of Electrical Engineering.

Mr. Richard Stevens: Ph.D candidate in Department of Systems Engineering (completed Ph.D degree in December, 1982).

Mr. Hiroyasu Ito: Ph.D candidate in Department of Systems Engineering (completed Ph.D degree in August, 1982).

Mr. Robert Gray: Ph.D candidate in Optical Sciences Center.

Mr. J. Su, first year Ph.D student in Electrical Engineering.

END

DATE
FILMED

4-84

DTIC